NOVEL THIN FILM

OPTICAL MODULATOR/TUNABLE RETARDER

A Thesis
Presented to
The Academic Faculty

By

David Keeling

In Partial Fulfillment
Of the Requirements for the Degree
Master of Science in Electrical Engineering

Georgia Institute of Technology

May 2007

NOVEL THIN FILM

OPTICAL MODULATOR/TUNABLE RETARDER

Approved by:

Dr. A. Rahman Zaghloul, Advisor
School of Electrical and Computer Engineering
Georgia Institute of Technology

Dr. P. Douglas Yoder
School of Electrical and Computer Engineering
Georgia Institute of Technology

Dr. W. Russell Callen Jr.
School of Electrical and Computer Engineering
Georgia Institute of Technology

Date Approved: April 5, 2007

ACKNOWLEDGEMENTS

I would like to thank my friends and family for their love and continued support. I would like to thank Dr. Zaghloul for his guidance, understanding, and most of all his patience with me. Finally, I would like to thank Wade Berzett for his suggestions, proofing, unmitigated criticism, and friendship.

TABLE OF CONTENTS

LIST OF TABLES

LIST OF FIGURES

NOMENCLATURE

$\overline{E}$	Electric field vector
$\overline{x}$	Orthogonal component of the electric field vector in the x direction
$\overline{y}$	Orthogonal component of the electric field vector in the y direction
t	Time
ω	Angular frequency
γ	Phase shift between x and y components of the electric field vector
θ	Angle of orientation for linearly polarized light
ϕ_0	Angle of incidence
ϕ_1	Angle of refraction into the film
ϕ_2	Angle of refraction into the substrate
ϕ_B	Brewster's angle
ϕ_C	Critical angle for total internal reflection
ϕ_{er}	Angle of incidence for an exact retarder
N_0	Refractive index of the ambient
N_1	Refractive index of the film
N_2	Refractive index of the substrate
ρ	Reflection ellipsometric function
ψ	Relative amplitude attenuation upon reflection
Δ	Relative phase shift upon reflection
X	Complex film-thickness exponential

r_{01p}	Fresnel coefficient of reflection at the ambient-film interface for parallel polarization
r_{01s}	Fresnel coefficient of reflection at the ambient-film interface for perpendicular polarization
r_{12p}	Fresnel coefficient of reflection at the film-substrate interface for parallel polarization
r_{12s}	Fresnel coefficient of reflection at the film-substrate interface for perpendicular polarization
$\Re_p$	Percentage reflected power for the parallel polarization
$\Re_s$	Percentage reflected power for the perpendicular polarization
δ_p	Phase shift upon reflection for the parallel polarization
δ_s	Phase shift upon reflection for the perpendicular polarization
d	Film thickness
d_j	Film thickness for a plus and minus j design
d_r	Reduced film thickness
R_p	Complex amplitude reflection coefficient for parallel polarization
R_s	Complex amplitude reflection coefficient for perpendicular polarization
D_{ϕ_0}	Film-thickness period
λ	Freespace wavelength
AIT	Angle-of-incidence tunable
CW	Clockwise
CCW	Counter-clockwise
CTC	Constant-thickness contour

CAIC	Constant-angle-of-incidence contour
SF	Subfamily
PMJ	Plus and minus j
PJEC	Plus-j-error contour
MJEC	Minus-j-error contour
PJA	Plus j angle-of-incidence
MJA	Minus j angle-of-incidence

SUMMARY

A reflection retarder is a device that induces a change in the phase between the parallel and perpendicular components, of the electric field, to the plane of incidence while maintaining the relative amplitudes. A film-substrate reflection retarder is a reflection retarder that only consists of a film-substrate system. Film-substrate reflection retarders have been previously studied in the negative, zero, and positive systems. The type of system is determined by the relationship between the refractive index of the ambient N_0, film N_1, and substrate N_2: if $N_1 < \sqrt{N_0 N_2}$, the system is negative; if $N_1 = \sqrt{N_0 N_2}$, the system is zero; if $N_1 > \sqrt{N_0 N_2}$, the system is positive. It has been determined that $N_1 \leq \sqrt{N_0 N_2}$ is the condition required to achieve reflection retarders, in general. Angle-of-incidence tunable (AIT) retarder designs have not been investigated for the zero system, but have been studied in the negative system. An exact retarder in the zero system only exists at a single angle of incidence and a corresponding single film thickness. By approximating the retarder condition to allow the relative amplitudes to be within 5% of the exact value of unity, it is possible to realize unique AIT retarders in the zero system: retarders that can be operated over a continuous range of angles of incidence resulting in a large range of phase shifts approaching 360°. It is possible to have multiple angles of incidence with a difference of π between their respective phase shifts. By inducing a phase shift of π, it is possible to modulate the polarization of light. By employing an approximation of the retarder condition, AIT retarder designs were developed. The design's tolerance to changes in design parameters is analyzed and discussed.

Chapter 1. Introduction

In this chapter, specific elementary optics concepts are discussed to provide a foundation for the topics presented in the following chapters. Additionally, previous work on optical devices is discussed. The devices discussed at the end of the chapter relate to the work presented in chapter 3. The scope of the paper is narrowed to a specific device of interest.

1.1 Polarization of an electromagnetic wave

Light is an example of an electromagnetic wave that propagates through space. The polarization of light is the contour traced by the electric field vector as a function of time at a fixed position in space.[1] Therefore, observing the electric field vector for a given period of time, the polarization of a given wave can be characterized by the contour of its electric field vector. The contour traced by this electric field vector over a single period can be linear, circular, or elliptical. The electric field vector $\overline{E}$ can be represented as

$$\overline{E} = \overline{x} + \overline{y}, \tag{1}$$

where $\overline{x}$ and $\overline{y}$ are the orthogonal components of the electric field vector Figure 1.1.1. The orientation of the electric field vector is represented here as a set of parametric equations:

$$\overline{x} = \overline{E}_x \cos(\omega t), \tag{2}$$

$$\overline{y} = \overline{E}_y \cos(\omega t + \gamma). \tag{3}$$

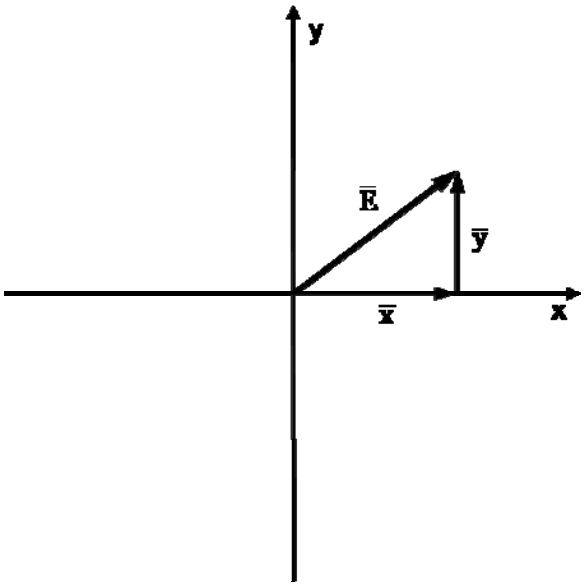

Figure 1.1.1 The electric field vector $\bar{E}$ is shown as the sum of its two orthogonal components $\bar{x}$ and $\bar{y}$.

$\bar{E}_x$ and $\bar{E}_y$ are the field amplitudes in their respective coordinate directions, ω is the angular frequency, t is time, and γ is the relative phase shift. The polarization of a beam of light can be determined by $\bar{E}_x$, $\bar{E}_y$, and γ. When γ=0, the beam is linearly polarized. When $\gamma = \pm \pi/2$ and $\bar{E}_x = \bar{E}_y$, the beam is circularly polarized. Linearly polarized light may be further classified by the orientation of the axis traced by the electric field vector, θ, where $-\pi/2 \le \theta \le \pi/2$ measured counter-clockwise from the positive x-axis, Fig. 1.1.2. Linearly polarized light with $\theta = \pm\pi/4$, implying $|\bar{E}_x| = |\bar{E}_y|$ from Eq. 4, and is of particular interest because it can be converted to circularly polarized light by inducing a $\pm\pi/2$ phase shift.

$$\theta = \arctan\left(\frac{\bar{E}_y}{\bar{E}_x}\right) \tag{4}$$

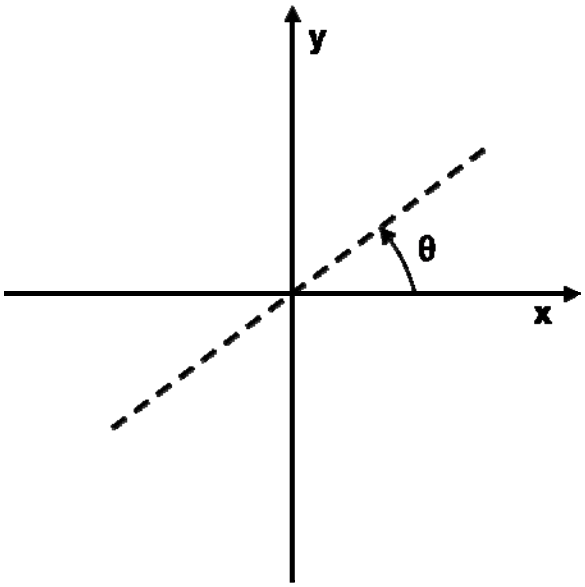

Figure 1.1.2 The axis for linearly polarized light is measured from the positive x-axis.

Similarly, circular and elliptical polarizations can be further classified by identifying the direction of rotation of the contour with time. If $\gamma = -\frac{\pi}{2}$, the electric field vector rotates clockwise (CW) and if $\gamma = \frac{\pi}{2}$, the electric field vector rotates counter-clockwise (CCW).[1]

1.2 Light at an interface

The refractive index of a material determines the speed of light in that material. When an electromagnetic wave encounters a change in refractive index at an interface between two different materials, part of the light is reflected backward and part of the light is transmitted through the interface into the new medium, Fig. 1.2.1. All materials considered here are linear, isotropic, transparent, and source free. To describe the

behavior of light at a given interface, the angle at which it is incident upon the interface must be considered. The angle of incidence ϕ_0 is measured from the line perpendicular to the surface at the point of reflection, therefore $0° \leq \phi_0 \leq 90°$, where normal incidence is at $\phi_0 = 0°$ and grazing incidence is at $\phi_0 = 90°$. The reflected beam returns from the interface at the same angle ϕ_0. However, the light that is transmitted through the interface changes direction to the angle of refraction ϕ_1, Fig. 1.2.1.

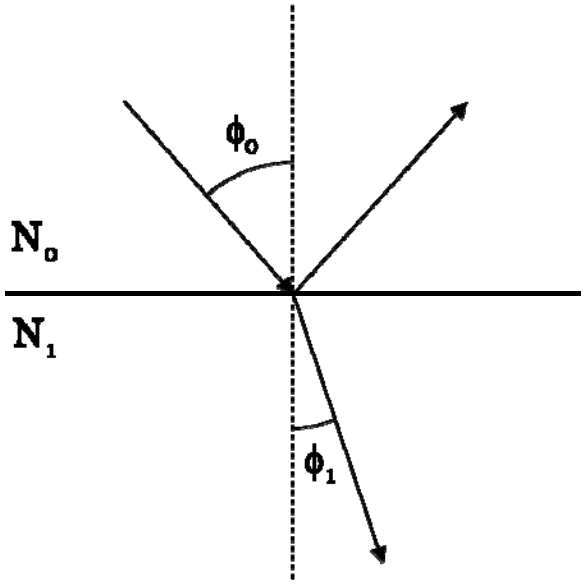

Figure 1.2.1 Light incident upon an interface at an angle ϕ_0 is reflected back at the same angle. The transmitted light is refracted at an angle ϕ_1. Using Snell's Law, $N_0 < N_1$, therefore $\phi_1 < \phi_0$.

The angle of incidence ϕ_0 and the angle of refraction ϕ_1 are related to the refractive index of the incident medium N_0 and to that of the encountered medium by Snell's Law:

$$N_0 \sin\phi_0 = N_1 \sin\phi_1 . \qquad (5)$$

The reflection at such an interface is characterized by the Fresnel coefficients of reflection:[2]

$$r_{01p} = \frac{N_1 \cos\phi_0 - N_0 \cos\phi_1}{N_1 \cos\phi_0 + N_0 \cos\phi_1} \tag{6}$$

$$r_{01s} = \frac{N_0 \cos\phi_0 - N_1 \cos\phi_1}{N_0 \cos\phi_0 + N_1 \cos\phi_1} \tag{7}$$

There is a different Fresnel coefficient for the two wave polarizations: where the electric field vector is parallel p or perpendicular s to the plane of incidence. By taking the square of the Fresnel reflection coefficient it is possible to find the percentage reflected power $\Re$ for a given polarization.

There are two different cases of reflection at an interface: internal and external. For the case of external reflection, $N_0 < N_1$, r_{01p}=0 at the Brewster angle ϕ_B, that is no p polarized light is reflected at $\phi_0 = \phi_B$. The s polarization experiences a phase shift δ_S=180° for all angles of incidence; the p polarization experiences a phase shift of δ_P=0° for $\phi_0 < \phi_B$ and δ_P=180° for $\phi_0 > \phi_B$, Fig 1.2.2. For the case of internal reflection, $N_0 > N_1$, there is a phase shift upon reflection that is dependent on the angle of incidence, Fig.1.2.3. Total internal reflection is a special condition for the internal reflection case where all of the light is reflected at the interface when $\phi_0 \geq \phi_C$.[2]

$$\phi_C = \arcsin(N_1 / N_0) \tag{8}$$

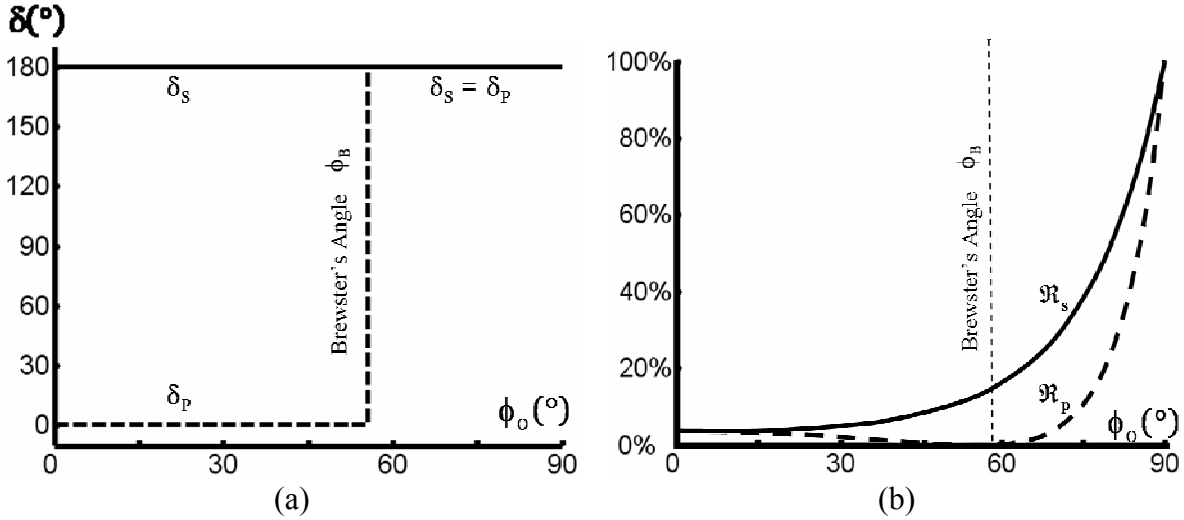

Figure 1.2.2 Phase shift and reflectances for the external reflection case where N_0 =1.0 and N_1 =1.46. Note that the percentage reflected power for the p polarization $\Re_p$ =0% at $\phi_0 = \phi_B$.

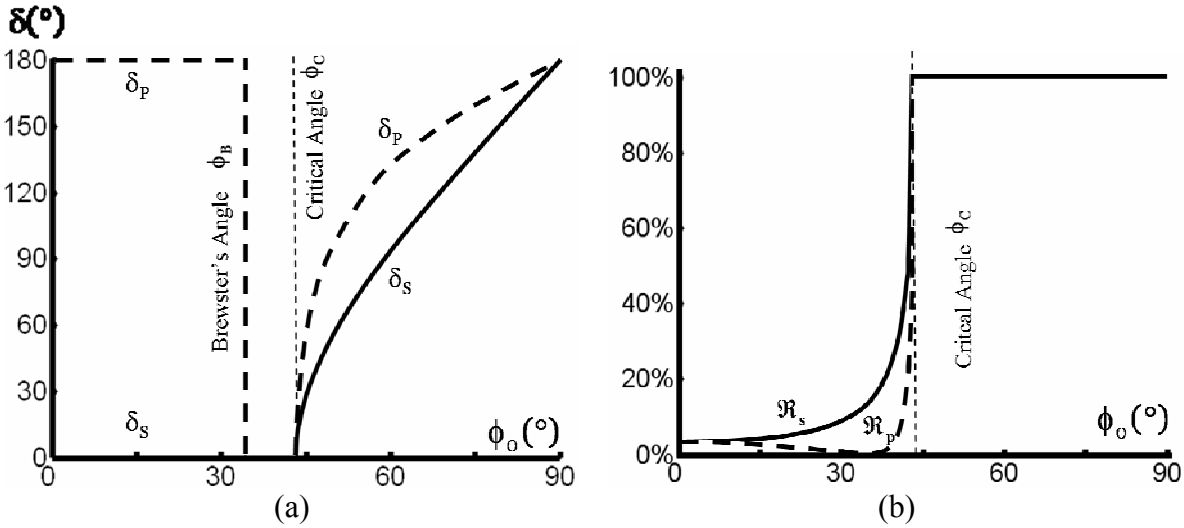

Figure 1.2.3 Phase shift and reflectances for the internal reflection case where N_0 =1.46 and N_1 =1.0. Note that the percentage reflected power for both polarizations $\Re_p = \Re_s$ =100% where $\phi_0 \geq \phi_C$.

1.3 Angle-of-Incidence-Controlled Modulator/Retarder Operation

An optical modulator is a general device that changes one or more parameters of light, in this case upon reflection. A specific type of optical modulator that is of interest is the reflection retarder. A reflection retarder is a device that maintains the relative amplitudes of the perpendicular s and parallel p components of the electric field vector upon reflection, while inducing a relative phase shift Δ between the p and s components. This device is used to manipulate light to desired polarization parameters. Reflection retarders may be divided into two groups based on the type of reflection used in the device: internal and external. Internal reflection retarders take advantage of phase shift upon reflection in the internal reflection case. Crystals such as the Fresnel Rhomb and other structures are frequently used as reflection retarders, specifically internal reflection retarders.[3] A film-substrate reflection retarder is an example of an external reflection retarder, where the device is simply a film deposited on a substrate, Fig. 1.3.1. Film-substrate reflection retarders are the focus of this thesis and from this point onward "retarder(s)" refers to film-substrate reflection retarder(s). An AIT retarder is a retarder that can be operated over a continuous range of angles of incidence resulting in a range of phase shifts upon reflection.

Designs for a film-substrate reflection retarder were suggested and demonstrated in Refs. 4-6. The designs were presented for the SiO_2-Si film-substrate system as an example. Ref. 7 presented a tunable reflection retarder using the MgF_2-Ag film-substrate system using the design procedure outlined in Refs. 4-6. This system as well as an MgF_2 film on other metallic substrates proved to be tunable with higher reflectances than the SiO_2-Si

system.[8,9] The external reflection retarder designs for the nonnegative film-substrate systems are presented and discussed in Refs. 8 and 9, and those for the negative film-substrate systems are presented and discussed in Refs. 4-6. The film-substrate systems have been divided into three types: negative $N_1 < \sqrt{N_0 N_2}$, zero $N_1 = \sqrt{N_0 N_2}$, and positive $N_1 > \sqrt{N_0 N_2}$. That is, the type of system is determined by the relationship of the refractive indices of the ambient N_0, film N_1, and substrate N_2.[8]

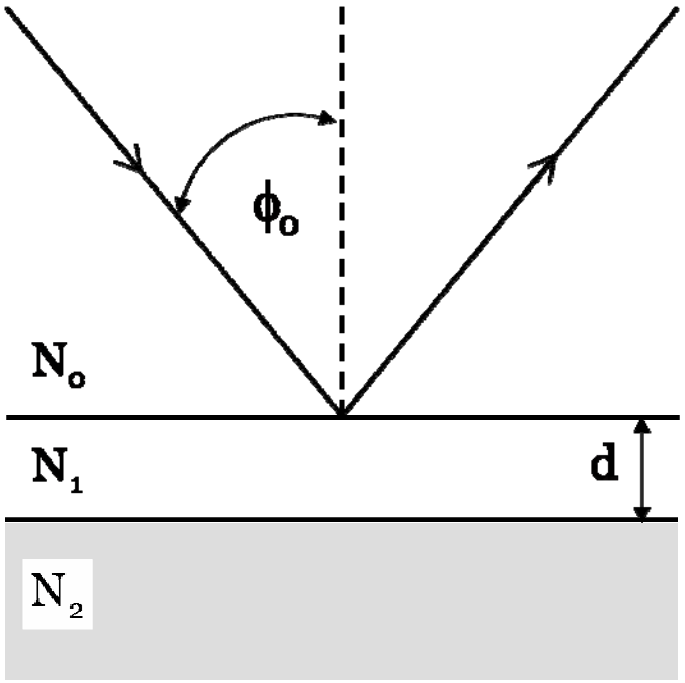

Figure 1.3.1: An electromagnetic wave is incident on a film-substrate system at an angle of incidence ϕ_0, where N_0, N_1, and N_2 are the refractive indices of the ambient, film, and substrate, respectively. The film thickness is d.

Chapter 2. Previous work – the ellipsometric function

This chapter presents the equations and planes used for analysis of film-substrate systems. The analysis is conducted for the zero film-substrate system only. The two primary contours used for analysis, the constant-angle-of-incidence contour (CAIC) and the constant-thickness contour (CTC) are presented and demonstrated in each plane.

2.1 The Ellipsometric Function

The ellipsometric function ρ represents the polarization behavior of the film-substrate system. ρ is the ratio of the complex amplitude reflection coefficients R_p and R_s, for parallel p and perpendicular s polarizations,

$$\rho = R_p / R_s = \tan(\psi)\exp(j\Delta). \tag{9}$$

R_p and R_s are written in the form,[4]

$$R_p = (r_{01p} + r_{12p}X)/(1 + r_{01p}r_{12p}X), \tag{10}$$

$$R_s = (r_{01s} + r_{12s}X)/(1 + r_{01s}r_{12s}X), \tag{11}$$

where r_{01p} and r_{01s} are given by Eqs. 6-7, and r_{12p}, , and r_{12s} are given by:

$$r_{12p} = \frac{N_2\cos\phi_1 - N_1\cos\phi_2}{N_2\cos\phi_1 + N_1\cos\phi_2}, \tag{12}$$

$$r_{12s} = \frac{N_1\cos\phi_1 - N_2\cos\phi_2}{N_1\cos\phi_1 + N_2\cos\phi_2}. \tag{13}$$

The film-thickness exponential function X is:

$$X = \exp[-j2\pi(d / D_{\phi_0})]. \tag{14}$$

D_{ϕ_0} is the film thickness period at which the value of ρ begins to repeat itself. Accordingly, ρ repeats itself at $d_1 = d + mD_{\phi_0}$, where d is any film thickness. By restricting d to the first period of D_{ϕ_0}, the reduced film-thickness subset d_r is realized,[4]

$$D_{\phi_0} = \frac{\lambda}{2\sqrt{N_1^2 - N_0^2 \sin^2 \phi_0}}, \tag{15}$$

and

$$0 < d_r \le D_{\phi_0}. \tag{16}$$

From the previous equations, it is clear that ρ is a function of the freespace wavelength λ, film thickness d, angle of incidence ϕ_0, and the refractive indices of the ambient N_0, film N_1, and substrate N_2. In practice, for a film-substrate system at a certain wavelength λ, N_0, N_1, and N_2 are all constants. In the lab, we can change the deposited film thickness d and the angle of incidence ϕ_o. Therefore, ρ is considered a function of only d and ϕ_0. In the next subsections we treat the ellipsometric function ρ as successive transformations from the $\phi_0 - d_r$ plane, to the complex X plane, and then to the complex ρ plane.[10]

2.2 The $\phi_o - d_r$ plane

The angle of incidence vs. the reduced film thickness plane is the first plane used for analysis. The reduced film thickness d_r is in the range of film thicknesses$(0, D_{\phi_0}]$. This is the simplest plane used, but it reveals much about the behavior of the film-substrate system. Note that D_{ϕ_0} does not depend on N_2, so the $\phi_0 - d_r$ plane can be used to analyze a system without considering the substrate material, Eq. (15). This implies that the $\phi_0 - d_r$ plane is the same for a negative, zero, and positive system with the same ambient and film indices. This plane shows D_{ϕ_0} and $D_{\phi_0}/2$ as a function of the angle of incidence ϕ_0, Fig. 2.2.1. The contours only depend on the wavelength λ, ambient index N_0, and film index N_1. The number of film-thickness subfamilies for a given system can be determined from the $\phi_0 - d_r$ plane. A subfamily (SF) is a set of continuous film thicknesses that have the same number of intersections with the $mD_{\phi_0}/2$ contours in the $\phi_0 - d_r$ plane. The intersections in the $\phi_0 - d_r$ plane correspond to intersections with the real axis in the complex X plane and the complex ρ plane. Therefore, SF1 is the set of film thicknesses ranging from (0, D_0/2] with zero intersections; SF2 ranges from (D_0/2, D_{90}/2) with one intersection; SF3 ranges from [D_{90}/2, D_0] with zero intersections; and SF4 ranges from (D_0, D_{90}) with one intersection, Fig. 2.2.1. One film thickness from each SF is presented for discussion, Fig. 2.2.2.[8,10]

The two primary contours used to analyze film-substrate systems can be shown in this plane; the constant-angle-of-incidence-contour (CAIC) and the constant-thickness-contour (CTC) are represented by a vertical line and horizontal line, respectively, Fig. 2.2.3. A CAIC holds the angle of incidence constant, while film thickness is changed from zero to D_{ϕ_0}. A CTC holds film thickness constant, while the angle of incidence is changed from 0° to 90°.

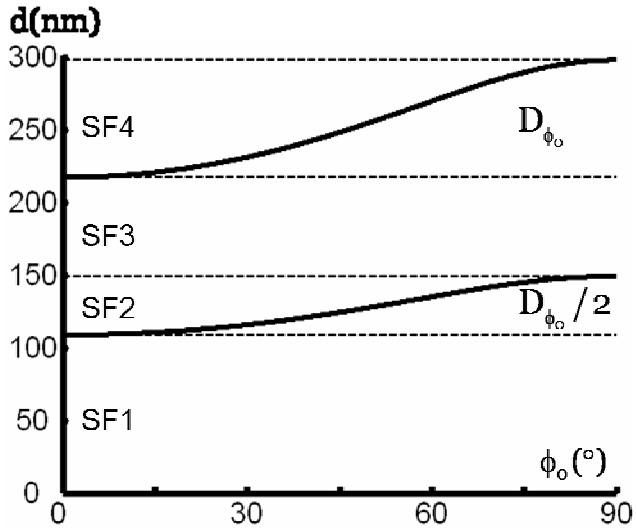

Figure 2.2.1 The angle of incidence vs. reduced film thickness plane for λ=632.8 nm, N_0=1.0, and N_1=1.46. This system has four subfamilies. Note that this plane does not use N_2, and is the same for a negative, zero, or positive system.

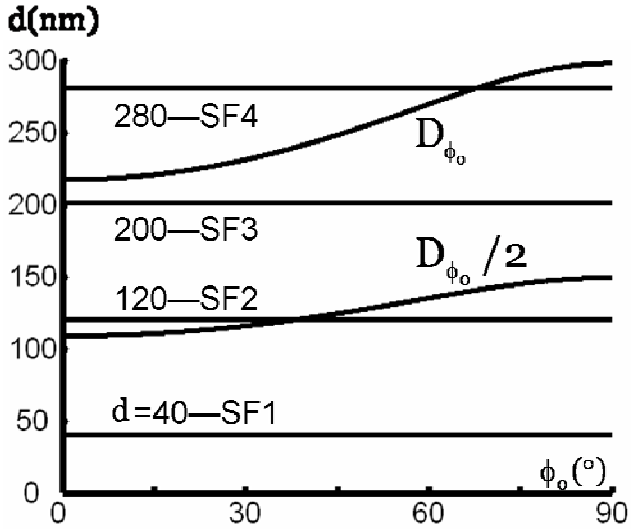

Figure 2.2.2 The reduced film thickness vs. angle of incidence plane for λ=632.8 nm, N_0=1.0, and N_1=1.46. This system has four subfamilies. One film thickness is shown from each subfamily for discussion.

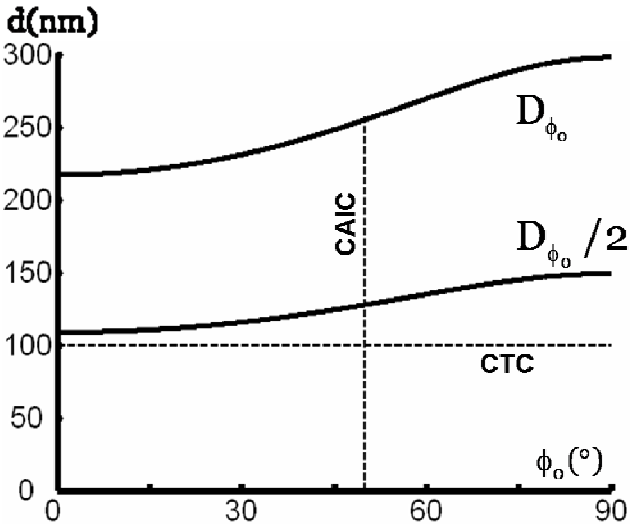

Figure 2.2.3 Same as Figure 2.2.1 except the horizontal line is a constant thickness contour (CTC) and the vertical line is a constant angle of incidence contour (CAIC). Note that the CAIC begins at 0 nm and terminates at D_{ϕ_0}

It is possible for a film-substrate system to have more than four SFs and that is determined by the ratio of N_0 to N_1. For such systems, the $\phi_0 - d_r$ plane shows multiples of $D_{\phi_0}/2$ up to the film thickness of D_{90}. However, one system with more than 4 SF's is used to show that designs presented in Ch. 3 do exist in these systems, Fig. 2.2.4.[10]

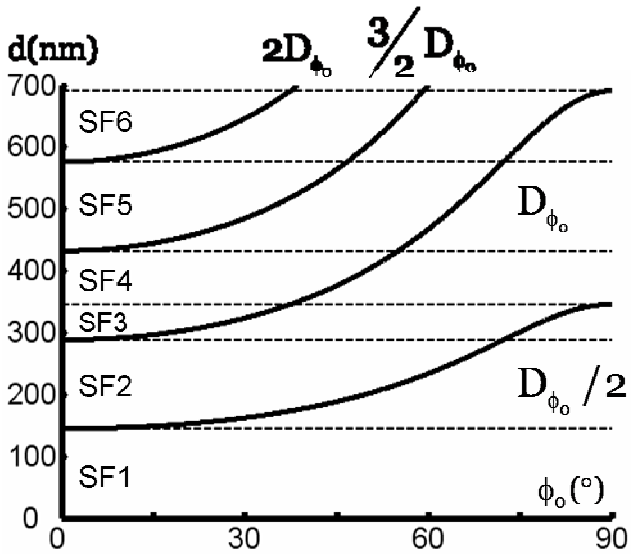

Figure 2.2.4 Same as Figure 2.2.1 except for N_1=1.1: there are six subfamilies.

2.3 X Plane

In the X plane a CAIC traces the unit circle in the clockwise direction for increasing the film-thickness at any angle of incidence. It starts at X= +1 where $d=0$ tracing the unit circle clockwise passing through X= -1 where $d = D_{\phi_0}/2$ and terminates at X= +1 where $d = D_{\phi_0}$, Fig. 2.3.1. CTCs trace an arc on the unit circle in the counter-clockwise direction for increasing angle of incidence. All SF1 CTCs are on the lower half of the

unit circle, all SF2 CTCs intersect the real axis at X=-1, all SF3 CTCs are on the upper half of the unit circle, and all SF4 CTCs intersect the real axis at X=+1, Fig 2.3.2. The CTCs in SF2 start on the upper half of the unit circle, pass through X=-1, and terminate on the lower half of the unit circle Fig. 2.3.4-2.3.5. The angle of incidence at which SF2 CTCs pass through X=-1 is the angle of incidence for the exact retarder design ϕ_{er}. Note that the complex X plane only takes into consideration λ, N_0, N_1, d, and ϕ_0. Thus a negative, zero, and positive film-substrate system with the same ambient and film indices share the same complex X plane.[9-11]

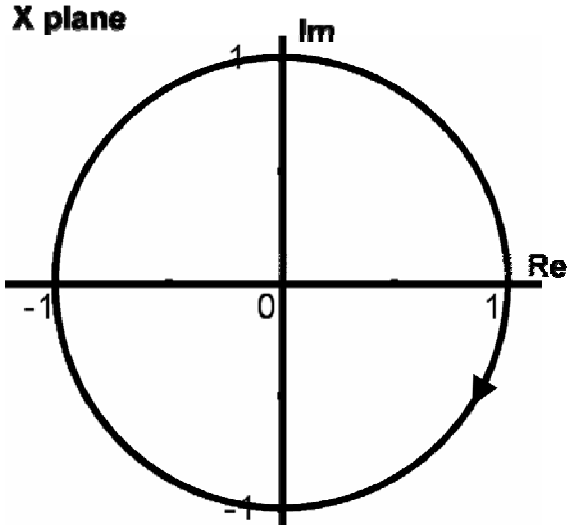

Figure 2.3.1 The CAIC transforms to a trace of the unit circle in the X plane. Note that this is the behavior for CAICs, regardless of ϕ_0. This general behavior is also true for any transparent film, for N_1 real.

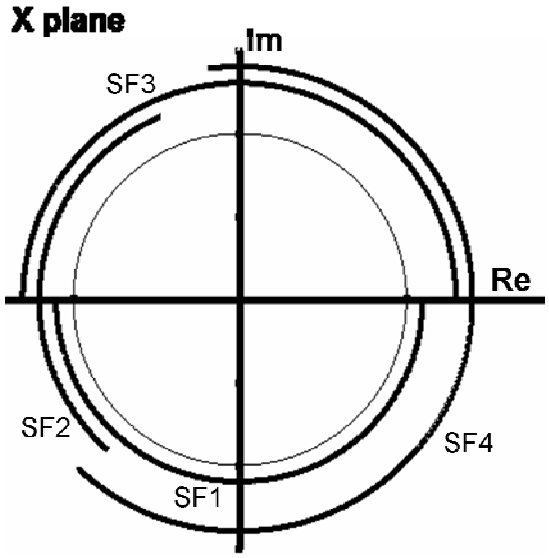

Figure 2.3.2 Range of CTCs for each SF. SF1 is on the lower half of the unit circle. SF2 intersects the real axis at X=-1. SF3 is on the upper half of the unit circle. SF4 intersects the real axis at X=+1.

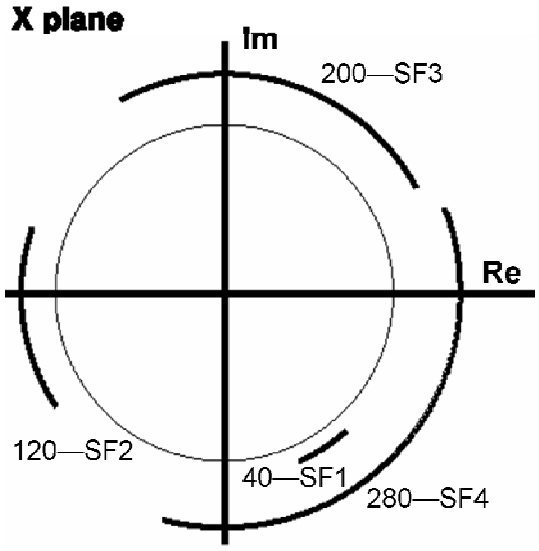

Figure 2.3.3 CTCs transform to arcs on the unit circle in the X plane. Example CTCs from Fig. 2.2.2 transform to arcs. Intersections with the real axis for SF2 and SF4 correspond to intersections with the mD_{ϕ_0} contours in the $\phi_0 - \mathrm{d}_\mathrm{r}$ plane.

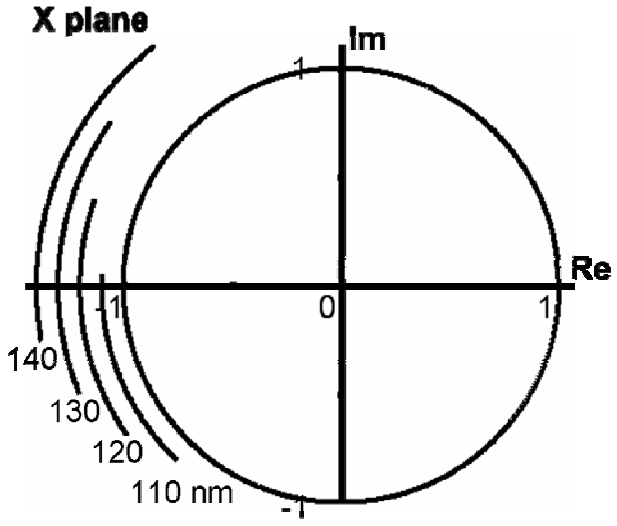

Figure 2.3.4 CTCs transform to arcs on the unit circle in the X plane. Multiple CTCs from SF2 are shown offset for clarity. All CTCs in SF2 intersect the point X=-1 in the X plane.

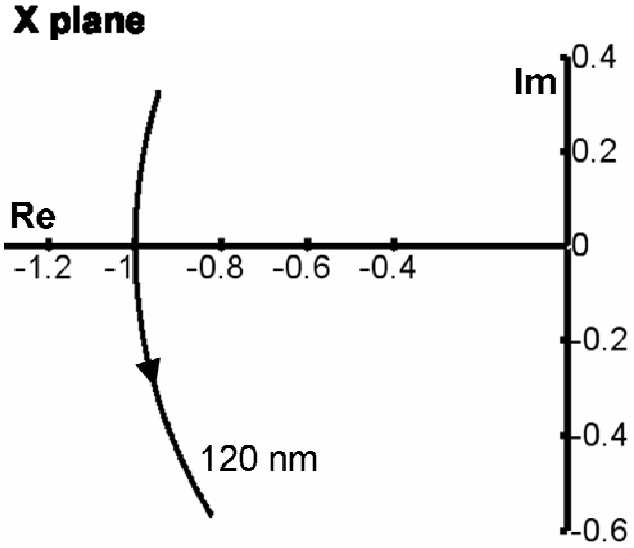

Figure 2.3.5 The 120 nm CTC from SF2 is shown to discuss the behavior of SF2 CTCs in the X plane. SF2 CTCs start on the positive imaginary half of the unit circle at ϕ_0 =0°, intersect X=-1 at ϕ_{er} (the angle of incidence of an exact retarder), and terminate on the negative imaginary half of the unit circle at ϕ_0 =90°.

2.4 Zero System Complex ρ Plane

2.4.1 Complex ρ Plane Constant-Angle-of-Incidence Contours (CAICs)

For the zero film-substrate system, the CAICs are contained within the complex unit circle, with the exception of an intersection at $\rho = \pm 1$.[8] The CAIC for normal incidence, $\phi_o = 0°$, maps to the point $\rho = -1$ and is the only CAIC to intersect this point: the contour collapses to a single point. CAICs for all other angles of incidence start on the real axis at $d = 0$ and trace clockwise and cross the real axis at the point $\rho = +1$ at $d = D_{\phi_0} / 2$ and terminate on the real axis at $d = D_{\phi_0}$. The size of these CAICs decreases as the angle of incidence increases, Fig. 2.4.1.1. The 90° CAIC is the point $\rho = +1$: the contour collapses to a single point.[10]

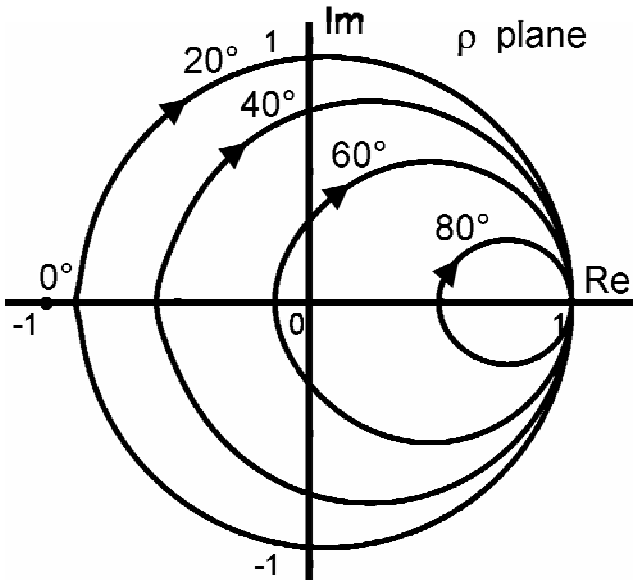

Figure 2.4.1.1 CAICs are shown for 0, 20, 40, 60, and 80°. All CAICs are centered on the real axis. The 0° CAIC is the point $\rho = -1$. All other CAICs share the common point $\rho = +1$ and decrease in size for increasing angle of incidence.

2.4.2 Complex ρ Plane-Constant-Thickness Contours (CTCs)

All CTCs begin at the point ρ=-1 and terminate at the point ρ=+1, Figs. 2.4.2.1-6. CTCs in the complex ρ plane are bound within the complex unit circle except at $\rho=\pm1$.[10] Retarder designs in the complex ρ plane are represented as an intersection with the unit circle. The intersection at ρ=-1 only occurs at ϕ_0=0°, normal incidence, and has no practical value. SF1 CTCs lie in the upper half of the complex unit circle, Fig. 2.4.2.1. For increasing film thickness in SF1, CTCs move away from the real axis. As the film thickness is increased from SF1 to SF2 the CTCs change direction corresponding to a change in the sign of X, Figs. 2.3.4-2.3.5. SF2 CTCs lie inside the lower half of the complex unit circle for $\phi_0 < \phi_{er}$, cross through ρ=+1 at $\phi_0 = \phi_{er}$, lie inside the upper half of the complex unit circle for $\phi_{er} < \phi_0 < 90°$, and terminate at ρ=+1 where $\phi_0 = 90°$, Fig. 2.4.2.2. For increasing film thickness in SF2, the loop formed where $\phi_{er} < \phi_0 < 90°$ decreases in size, Fig. 2.4.2.2. As the film thickness is increased from SF2 to SF3 the loop in SF2 collapses and vanishes at $d = D_{90}/2$. SF3 CTCs lie inside the lower half of the complex unit circle. For increasing film thickness in SF3, CTCs move closer to the real axis, Fig 2.4.2.3. As the film thickness is increased from SF3 to SF4, CTCs change direction corresponding to a change in the sign of X, Figs. 2.3.2-2.3.3. SF4 CTCs start inside the upper half of the complex unit circle, cross the real axis, and move into the negative half of the complex unit circle, Fig. 2.3.2.4. The dashed portion of SF4 CTCs in Fig. 2.3.2.4 is a projection into SF1 corresponding to the portion of SF4 CTCs that lies above the D_{ϕ_0} contour in the $\phi_0 - d_r$ plane, Fig.2.2.2.[10]

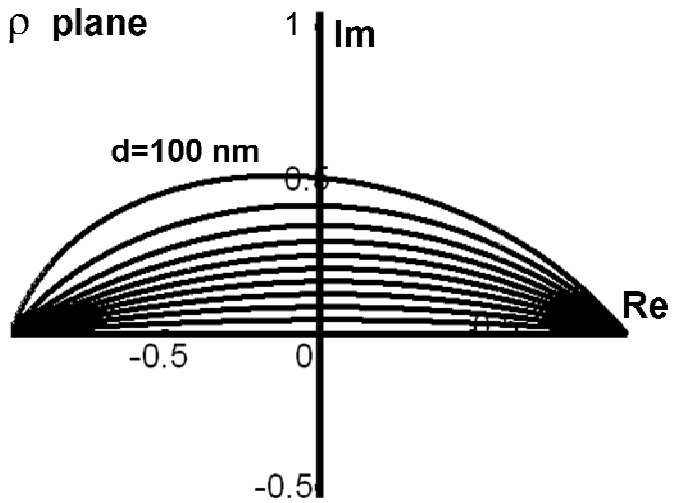

Figure 2.4.2.1 SF1 CTCs for the 1.46 zero system are in the upper half of the plane. The contours range from 0 to 100 nm in 10 nm increments.

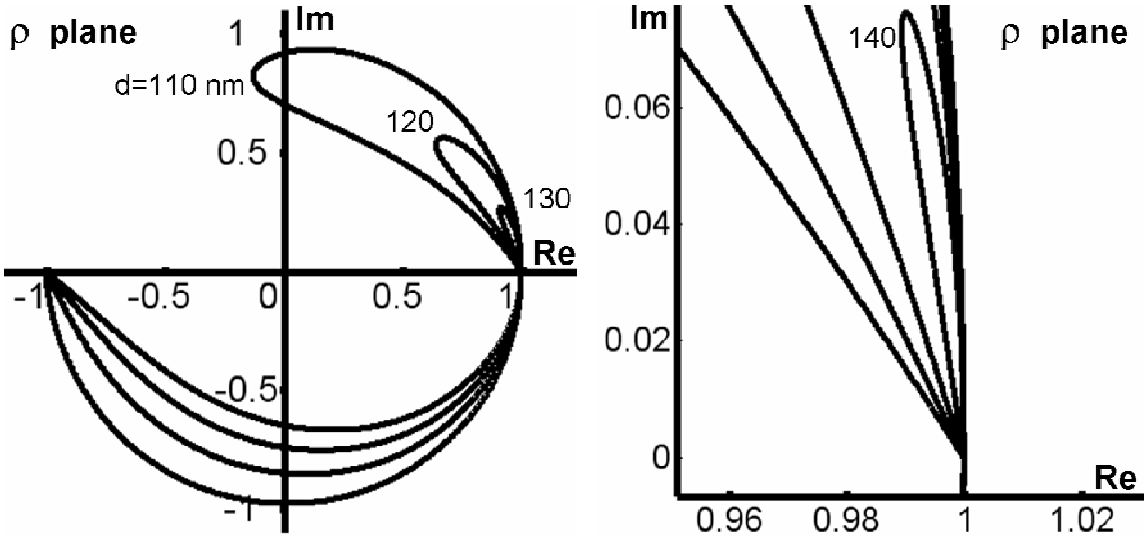

(a) (b)

Figure 2.4.2.2 SF2 CTCs are shown for 110, 120, 130, and 140 nm. All SF2 CAICs start at ρ=-1, move into the negative imaginary half of the complex unit circle, intersect ρ=+1 at ϕ_{er}, move into the positive imaginary half of the complex unit circle, and loop around to terminate at ρ=+1. The loop for the 110nm CTC is the largest and decreases in size for each succeeding CTC. A similar pattern exists for the intersection with the negative imaginary axis: the 110 nm CTC has the lowest intersection (largest arc) and the 140 nm CTC has the highest intersection (smallest arc). The 140 nm CTC loop is shown in (b) with the other CTCs for reference.

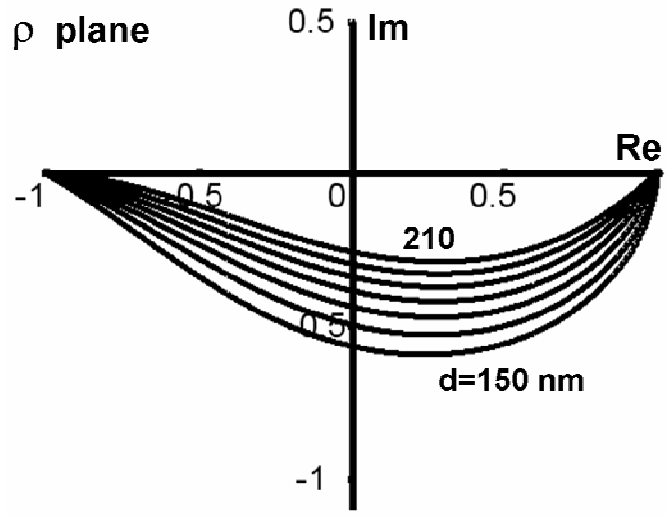

Figure 2.4.2.3 SF3 CTCs are shown from 150 to 210 nm in 10 nm increments. SF3 CTCs are entirely in the lower half of the plane.

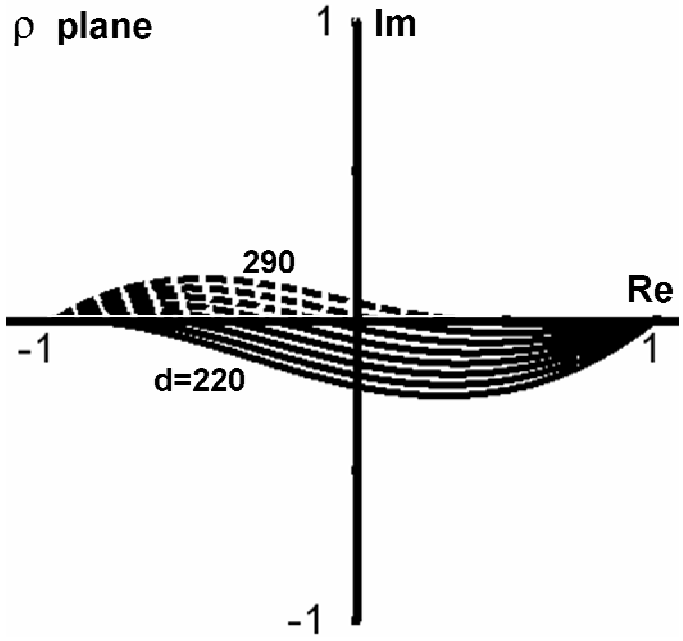

Figure 2.4.2.4 SF4 CTCs are shown from 220 to 290 nm in 10 nm increments. All SF4 CTCs cross the real axis as a projection onto the d =0 nm CTC. The dashed portion of the CTCs is where they are projected onto SF1 CTCs.

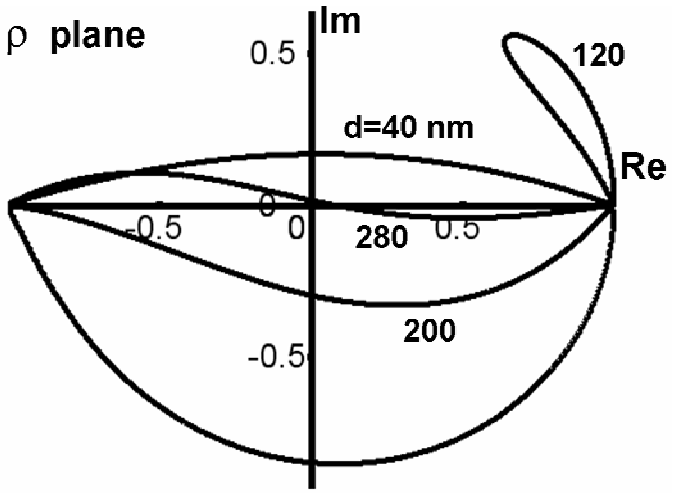

Figure 2.4.2.5 Example CTCs from Fig. 2.2.2. SF1 CTCs are in the upper half of the plane. When the film thickness crosses into SF2 the CTC starts moving into the lower half of the plane due to a change in the sign of X, Fig. 2.3.5. SF2 CTCs pass through $\rho = +1$ at $\phi_0 = \phi_{er}$. SF3 CTCs are in the lower half of the plane. SF4 CTCs move into the upper half of the plane and cross the real axis into the lower half of the plane.

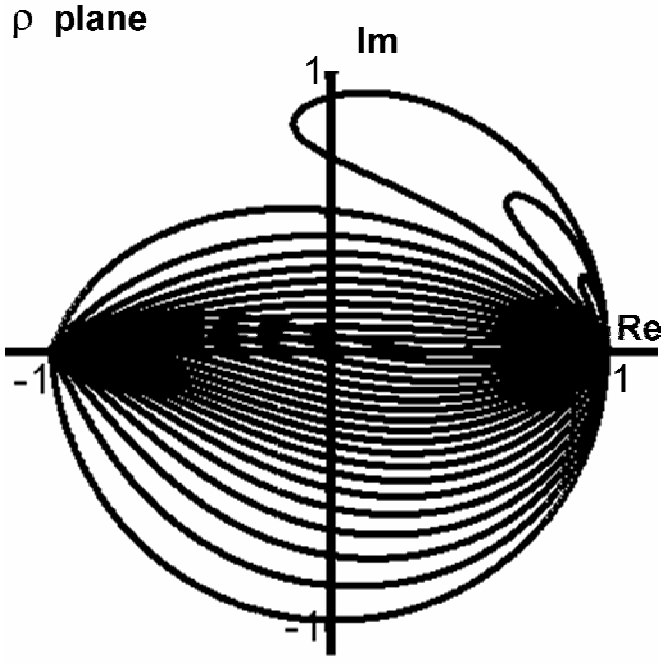

Figure 2.4.2.6 All SFs CTCs for the 1.46 zero system. The only intersections with the unit circle are at $\rho = \pm 1$.

Chapter 3. Plus and Minus J

In this chapter, the optical modulator/tunable retarder is presented as a plus and minus j device (PMJ). First, the approximation used to design the PMJ device is introduced and discussed. Next, properties of the PMJ devices are discussed. The PMJ design contours, which show all possible PMJ designs for a given film-substrate system, are presented and discussed. A design algorithm is presented and is also illustrated with three example designs. Finally, device sensitivity to input parameters, and device performance are presented and discussed.

3.1 PMJ Approximation

An ideal plus and minus j (PMJ) device is a tunable retarder with a phase shift of +90° and -90°, as changed with the angle of incidence. This allows for linearly polarized light with $\theta = 45°$ to be reflected as circularly polarized light with a clockwise or counter-clockwise rotation, $\rho = +j$ and $\rho = -j$, respectively. However, in the zero system it is not possible to intersect $\rho = +j$ or $\rho = -j$ because the magnitude of ρ is always less than one except at $\rho = \pm 1$.[8,10] However, to design the device practically, the value of ρ only needs to be close to $\pm j$ to function within an acceptable tolerance. Allowing for a margin of error in the magnitude of ρ of ±5% the required designs are achieved. This establishes the +j-error contour (PJEC) and the –j-error contour (MJEC): a circle at the desired value with a radius of 0.05. By choosing an area of acceptable designs it allows more design flexibility. The allowed error of 5% is an arbitrary example used for discussion; a designer could choose the acceptable error for a particular application.

3.2 Properties of PMJ

PMJ designs only occur in the lower thicknesses of SF2. As the film-thickness is increased in SF2, the loop gets smaller and does not intersect the PJEC, Fig. 2.4.2.2. For the smallest SF2 film thickness of a film-substrate system, the intersections of the ρ CTC with the imaginary axis are the closest points to plus and minus j, Fig. 3.2.1. It exhibits the largest loop for the N_1 =1.1 zero film-substrate system. However, at this thickness, the angles of incidence for the plus and minus j are too small, less than 1°. The algorithm of Section 3.3 yields more practical designs by pre-selecting the angle of incidence for +j operation. The smallest SF2 CTC exhibits the largest loop and the maximum phase retardation Δ in SF2 for a given film-substrate system. For systems of increasing index, maintaining the zero system, the maximum Δ decreases as N_1 increases, Fig. 3.2.2. PMJ designs are not possible in a zero film-substrate system where $N_1 / N_0 \geq 2.12$, using a 5% margin of error; the characteristic loop of SF2 CTCs no longer intersects the PJEC, Figs. 3.2.3-3.2.4.

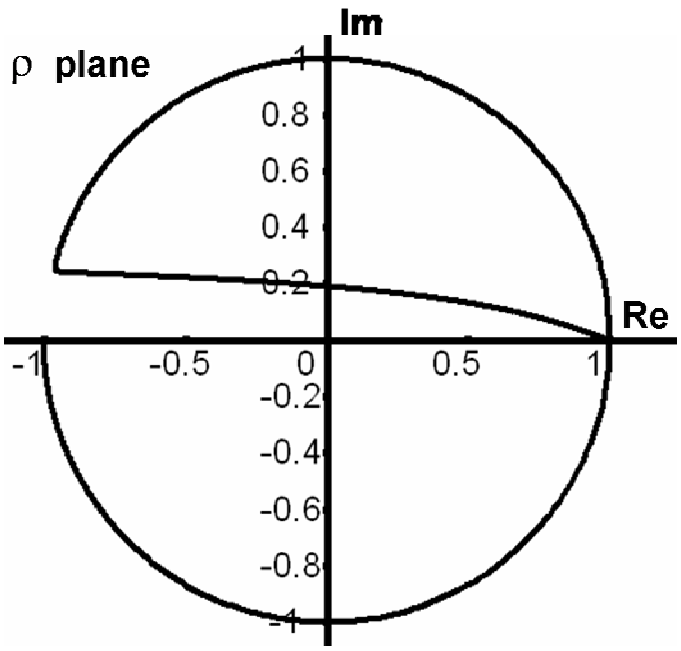

Figure 3.2.1 First film thickness of SF2 CTC for the N_1=1.1 zero film-substrate system, where $d \approx 134.8$ nm. This CTC has the largest loop and is the closest to the complex unit circle. As the film thickness is increased, the loop gets smaller and the CTC moves further away from the complex unit circle. The portion of the CTC that nearly traces the complex unit circle is spanned in $0° \le \phi_0 < 2°$. The maximum phase retardation for this system is Δ=166.1°, corresponding to the tip of the loop. As the film thickness increases, the loop decreases in size and Δ decreases.

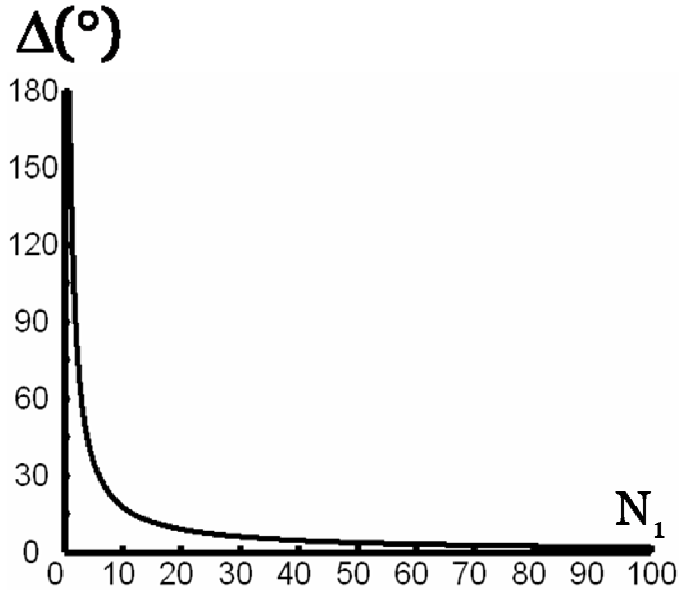

Figure 3.2.2 The maximum phase retardation for zero systems, taken from the first CTC of SF2. Note that $1 < N_1 \leq 100$, maintaining the zero system, and the origin is only shown for reference. As N_1 approaches N_0, the maximum Δ approaches 180°. As N_1 approaches ∞, the maximum Δ approaches 0°

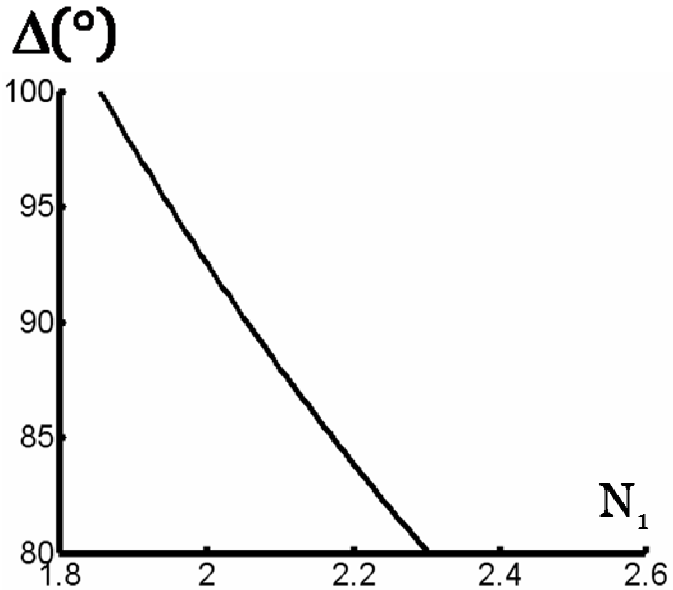

Figure 3.2.3 Same as in Fig. 3.2.2 ,except zoomed in to show Δ near N_1 =2.12.

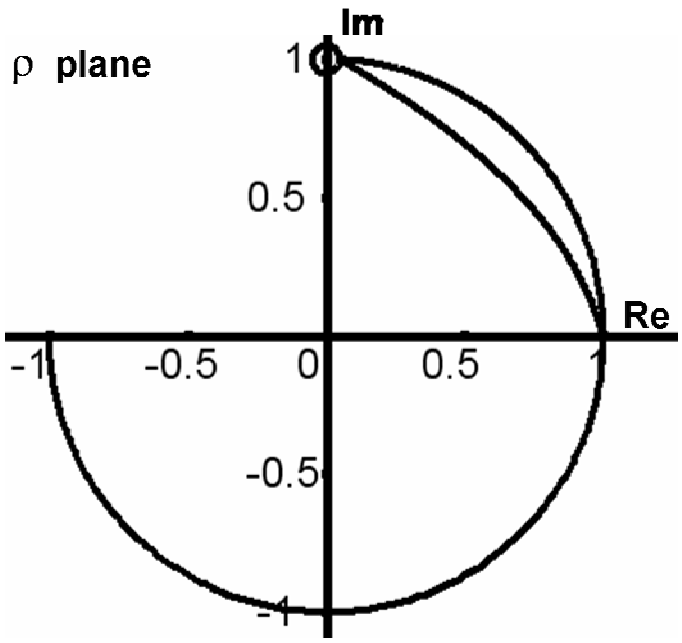

Figure 3.2.4 First film thickness CTC of SF2 for the N_1=2.12 zero system, where $d \approx 74.3$ nm. The maximum phase retardation for this system is $\Delta = 86.8°$. Note that the CTC grazes the PJEC and increasing N_1, maintaining the zero system, results in no intersections with the PJEC.

3.3 PMJ Design Contours

By calculating the film thickness intersection of CAICs with PJEC and MJEC starting at $\phi_0 = 0°+$ and increasing ϕ_0 until there are no intersections, the PMJ design contours are obtained, Figs. 3.3.1-3.3.5. Calculating the film thickness intersections with the PJEC and the MJEC are illustrated in Figs. 3.3.1 and 3.3.2, respectively. The design contours are a representation of all possible designs for a given system. By introducing these design contours as a guide, the design of a PMJ device for a given zero system is simplified. It establishes all possible designs for a given system. The algorithm in section 3.4 is used to select design points in the middle of the PMJ design contours by averaging the points on those design contours. PMJ design contours for the example

systems in the illustrated algorithm are shown in figures 3.3.3-3.3.5: for N_0=1; N_1=1.1, 1.46, and 1.697; N_2=1.21, 2.1316, 2.8798, respectively. A total of three example systems. Figs. 3.3.3-3.3.5 show the design contours for +j and –j which encompass the angle of incidence and film thickness regions where ρ is inside the PJEC or the MJEC. The –j design contour is above the +j one. It has a lower angle of incidence at a given film thickness ranges, Figs. 3.3.3-3.3.5. The –j design contour continues into a thickness region above the maximum film thickness of the +j design contour. This is due to the SF2 CTC loop not intersecting the PJEC, while the MJEC is still intersected by the CTC, Figs. 3.3.3-3.3.5. The –j design contour is narrower than the +j one because it is more sensitive to changes in film thickness and angle of incidence. The –j design contour is widest beyond the maximum film thickness for the +j contour, where the range of the angle of incidence for –j operation is larger, Figs. 3.3.3-3.3.5. Increasing N_1, maintaining the zero system, causes several changes to the PMJ design contours: widening the PMJ design contours, increasing the range of ϕ_0 for PMJ designs, and increasing the difference between the angle of incidence for +j operation (PJA) and the angle of incidence for –j operation (MJA) , Figs. 3.3.3-3.3.5.

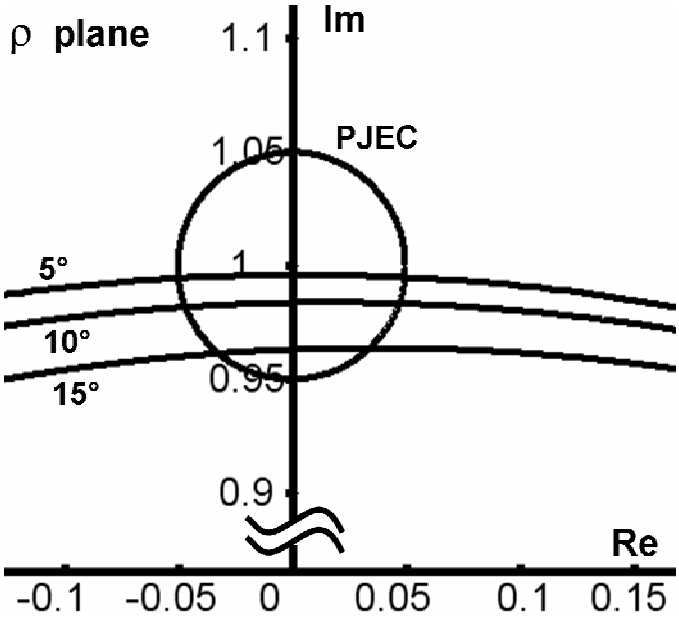

Figure 3.3.1 CAIC intersections with the PJEC calculated for the N_1 =1.46 zero system. The film thickness intersection for the 5°, 10°, and 15° CAICs are 108.449 nm ≤ d ≤ 108.4579 nm, 108.7182 nm ≤ d ≤ 108.7553 nm, and 109.1497 nm ≤ d ≤ 109.2122 nm, respectively.

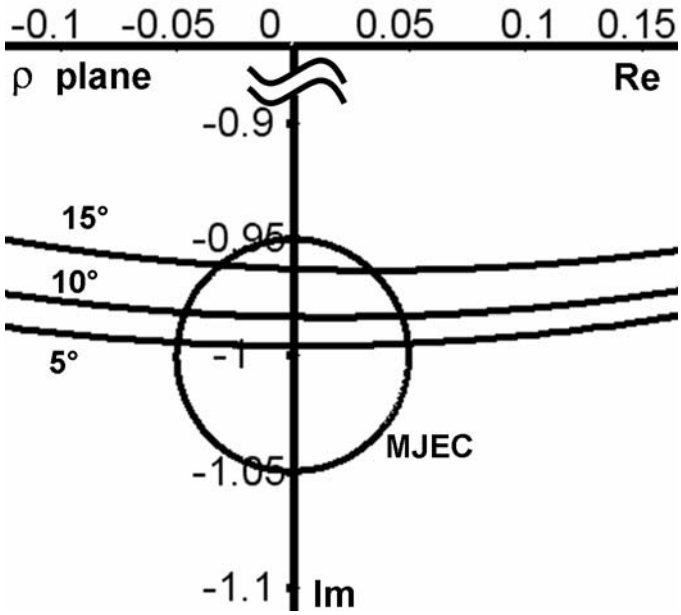

Figure 3.3.2 CAIC intersections with the MJEC calculated for the N_1 =1.46 zero system. The film thickness intersection for the 5°, 10°, and 15° CAICs are 108.4522 nm ≤ d ≤ 108.455 nm, 108.7307 nm ≤ d ≤ 108.7428 nm, and 109.1678 nm ≤ d ≤ 109.1945 nm, respectively.

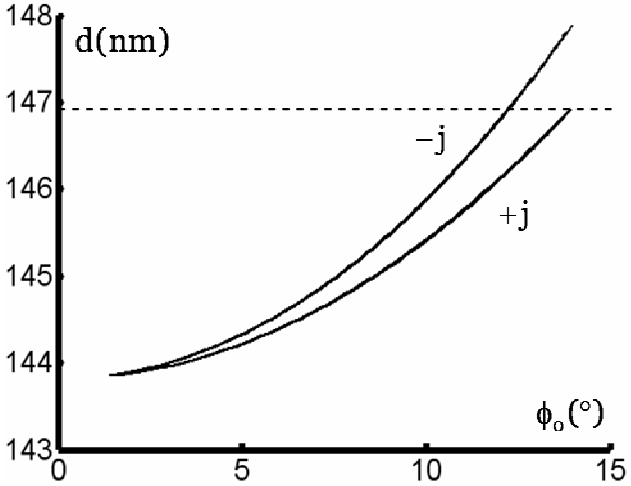

Figure 3.3.3 The plus and minus j design contours for the 1.0/1.1/1.21 zero system. The designs exist in the area between the minimum and maximum boundaries. Note that the –j contour spans a larger thickness range than the +j one. The dashed horizontal line signifies the maximum thickness at which PMJ designs exist. One way to use the design contours is to select a film thickness and the angles of operation for –j and +j are found from the figure.

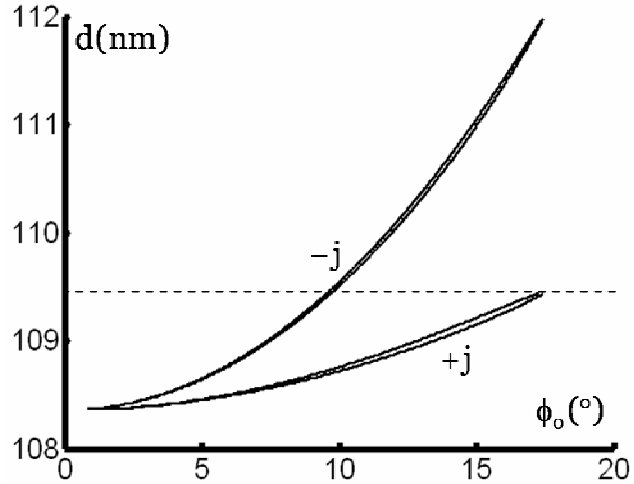

Figure 3.3.4 Same as in Figure 3.3.3, but for the 1.0/1.46/2.1316 zero system. The PMJ design contours are wider than those in Fig. 3.3.3 and have a larger range of ϕ_0.

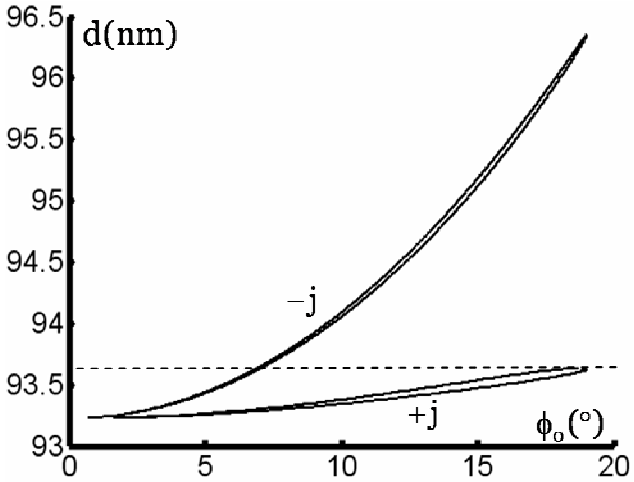

Figure 3.3.5 Same as in Figure 3.3.1, but for the 1.0/1.697/2.8798 zero system. The PMJ design contours are wider than those in Figs. 3.3.3 and 3.3.4 and have a larger range of ϕ_0.

3.4 PMJ Design Algorithm

This design algorithm uses N_1 and the angle of incidence ϕ_0 for +j operation (PJA) as inputs and provides film thickness and the angle of incidence for –j operation (MJA).

1. Select a zero film-substrate system, with a film-ambient ratio $N_1 / N_0 \leq 2.12$, Fig. 3.2.4.
2. Select the angle of incidence for +j operation (PJA). 5°< PJA <15° is suggested because designs for this range are available in most systems.
3. Calculate the film thickness intersections of the PJA CAIC with the PJEC, Sec. 3.3.
4. Calculate the average thickness (d_j) of the thicknesses obtained in step 3.
5. Calculate the angle of incidence intersections of the CTC for d_j with the MJEC.
6. Calculate the average of the angles from step 5 to yield the angle of incidence for –j operation MJA.
7. Calculate PJA-MJA. This is the change in the angle of incidence to transition from +j operation to –j operation, and vice versa. This is a practical consideration for the designer. Acceptable values are determined by the designer.
8. If the difference between PJA and MJA, calculated in step 7, is too large, select a zero system with a lower N_1 /smaller PJA, or vice versa, and go back to step 1. Systems with a smaller value of N_1 have a smaller difference between PJA and MJA, Sec. 3.3. A smaller value of PJA yields a lower film thickness, decreasing the difference between PJA and MJA, Figs. 3.3.3-3.3.5.

3.5 Example Zero Systems

Three different zero system examples are presented to illustrate PMJ designs. N_0=1 in each system; N_1=1.1, 1.46, and 1.697 and N_2=1.21, 2.1316, and 2.8798, respectively. By analyzing these different systems, trends in the designs' behavior are developed. The N_1=1.1 zero system was chosen because it is an example of a film-substrate system with more than four SFs. The N_1=1.46 is the film index for SiO_2 at λ=632.8 nm. The N_1=1.697 zero system represents a high index glass at λ=632.8 nm.

3.6 Illustrated Algorithm

To illustrate the algorithm, the results of each step of the algorithm are presented in this section; one design example for each of the three zero systems. The zero systems are given in Sec. 3.5, therefore step 1 is complete.

2. Select PJA=10°.
3. Calculate the film thickness intersections of the PJA CAIC with the PJEC.
    a. System 1: 145.403≤d≤145.421 nm
    b. System 2: 108.719≤d≤108.751 nm
    c. System 3: 93.342 ≤d≤93.376 nm
4. Calculate the average film thickness (d_j) of the thicknesses obtained in step 3.
    a. System 1: 145.4123 nm
    b. System 2: 108.7368 nm
    c. System 3: 93.3592 nm

5. Calculate the angle of incidence intersections of the d_j CTC with the MJEC.

   a. System 1: $8.7911° \le \phi_0 \le 8.8362°$

   b. System 2: $5.6798° \le \phi_0 \le 5.7744°$

   c. System 3: $3.9752° \le \phi_0 \le 4.0583°$

6. Calculate the average of the angles from step 5 to yield the angle of incidence for –j operation MJA.

   a. System 1: 8.8136°

   b. System 2: 5.7271°

   c. System 3: 4.0168°

7. Calculate PJA-MJA.

   a. System 1: 1.1864°

   b. System 2: 4.2729°

   c. System 3: 5.9832°

8. The results for PJA-MJA are acceptable for the example.

3.7 Sensitivity Analysis and Performance

For completeness, the different designs' sensitivity to changes in the angle of incidence ϕ_0, in the film thickness d, in the film index N_1, and in the substrate index N_2 are considered. The designs shown in Table 3.7.1 are analyzed for sensitivity. The designs chosen are examples of the suggested range of PJA for the three example systems.

Table 3.7.1 The following designs are used in the sensitivity analysis. Note that system 1 does not have a design for PJA=15° because that design is not possible for that system.

System	Indices	PJA (°)	MJA (°)	d (nm)
1	1.0/1.1/1.21	5	4.4201	144.216
		10	8.8136	145.4123
2	1.0/1.46/2.1316	5	2.8989	108.4534
		10	5.7271	108.7368
		15	8.4143	109.1809
3	1.0/1.697/2.8798	5	2.0595	93.259
		10	4.0168	93.3592
		15	5.7617	93.5032

3.7.1 Angle of Incidence

The angle of incidence sensitivity applies to both PJA and MJA at their respective angles of operation. A change in ϕ_o results in a change in Δ, but negligibly affects $\tan\psi$ in the operation of PMJ, as the design is a tunable one. Sensitivity to changes in ϕ_o for MJA is identified in step 5 of the algorithm by calculating the angle of incidence intersections of the d_j CTC with the MJEC. PJA sensitivity to changes in ϕ_o is found by calculating the angle of incidence intersections with the PJEC for the d_j CTC. Tolerances are also found by referring to the PMJ design contours Figs 3.3.3-3.3.5. A larger range of ϕ_o satisfies the approximation for higher design values of PJA, but the range tapers off toward the maximum PJA of a system. MJA is more sensitive to changes in ϕ_o than PJA, Table 3.7.1.1. This can be attributed to the nature of SF2 CTCs. An SF2 CTC moves from ρ=-1 to ρ=+1 (Δ=180° to Δ=0°) in the span of ϕ_{er} degrees. ϕ_{er} is small for all PMJ designs; a small change in the angle of incidence results in a large change in Δ. A

larger range of ϕ_o is within the 5% tolerance for systems with a higher value of N_1, but the range tapers off to the limit of N_1 =2.12, Figs 3.3.3-3.3.5.

Table 3.7.1.1 The sensitivity of the example designs for ϕ_o. Note that for higher values of PJA the ranges increase. Also note that the tolerances improve from system 1 to system 2 and from system 2 to system 3. MJA is more sensitive to a change in ϕ_o than PJA. This trend is also apparent from figures 3.3.3-3.3.5.

System	PJA (°)	PJA Min (°)	PJA Max (°)	PJA Range (°)	MJA (°)	MJA min (°)	MJA max (°)	MJA Range (°)
1	5	4.9828	5.0176	0.0348	4.4201	4.4081	4.4321	0.024
	10	9.9689	10.0322	0.0633	8.8136	8.7911	8.8362	0.0451
2	5	4.8807	5.1301	0.2494	2.8989	2.8749	2.9228	0.0479
	10	9.7545	10.2626	0.5081	5.7271	5.6798	5.7744	0.0946
	15	14.6903	15.3039	0.6136	8.4143	8.3459	8.4827	0.1368
3	5	4.7167	5.3463	0.6296	2.0595	2.0382	2.0808	0.0426
	10	9.3848	10.76	1.3752	4.0168	3.9752	4.0583	0.0831
	15	14.0152	16.087	2.0718	5.7617	5.7022	5.8213	0.1191

3.7.2 Film thickness

The film thickness sensitivity affects both +j and –j design points simultaneously as they both depend on the same film thickness. Sensitivity to changes in film thickness is identified in step 3 of the algorithm for the +j design point by calculating the film thickness intersections of the PJA CAIC with the PJEC. It is determined by calculating the MJA CAIC film thickness intersections with the MJEC, Fig. 3.3.2. The –j design point is more sensitive to changes in film thickness than the +j design point, Sec. 3.3. It can bee seen on the PMJ design contours that the –j contour is narrower than the +j contour and has a greater slope, Figs. 3.3.3-3.3.5. Note that the –j design contour has its thickest region above the thickness cutoff for PMJ designs, Figs. 3.3.3-3.3.5. The

sensitivity for the –j design point is the restricting case when considering changes in film thickness, Table 3.7.2.1. A larger range of d satisfies the approximation for systems with a higher value of N_1, but the range tapers off to the limit of N_1=2.12, Fig. 3.2.4.

Table 3.7.2.1 The sensitivity of the example designs for d. Note that for higher values of PJA the ranges increase. Also note that the tolerances improve from system 1 to system 2 and from system 2 to system 3. –j is more sensitive to a change in d than +j. This trend is also apparent from figures 3.3.3-3.3.5.

System	PJA (°)	d (nm)	+j dmin (nm)	+j dmax (nm)	+j Range (nm)	-j dmin (nm)	-j dmax (nm)	-j Range (nm)
1	5	144.216	144.2149	144.217	0.0021	144.2149	144.217	0.0021
	10	145.4123	145.4032	145.4214	0.0182	145.4052	145.4193	0.0141
2	5	108.4534	108.449	108.4579	0.0089	108.4522	108.455	0.0028
	10	108.7368	108.7182	108.7553	0.0371	108.7307	108.7428	0.0121
	15	109.1809	109.1497	109.2122	0.0625	109.1678	109.1945	0.0267
3	5	93.259	93.2548	93.2632	0.0084	93.2584	93.2597	0.0013
	10	93.3592	93.3421	93.3763	0.0342	93.3565	93.3618	0.0053
	15	93.5032	93.4707	93.5358	0.0651	93.4977	93.509	0.0113

3.7.3 Film index

The film index sensitivity analysis allows consideration for changes in N_1, keeping N_2 unchanged. This causes an immediate change from a zero to a negative or a positive system. Increasing N_1 results in a positive system; where decreasing N_1 results in a negative system. Despite the change in system category, the negative and positive regions analyzed are very close to the zero system and thus still have PMJ designs, Fig. 3.7.3.1. The –j design point is more sensitive to a change in N_1 than the +j design point, Table 3.7.3.1. Thus, the sensitivity for the –j design point is the restricting case for designs when considering changes in film index. A larger range of N_1 satisfies the

approximation for systems with a higher value of N_1, but the range tapers off to the limit of N_1=2.12, Fig. 3.2.4.

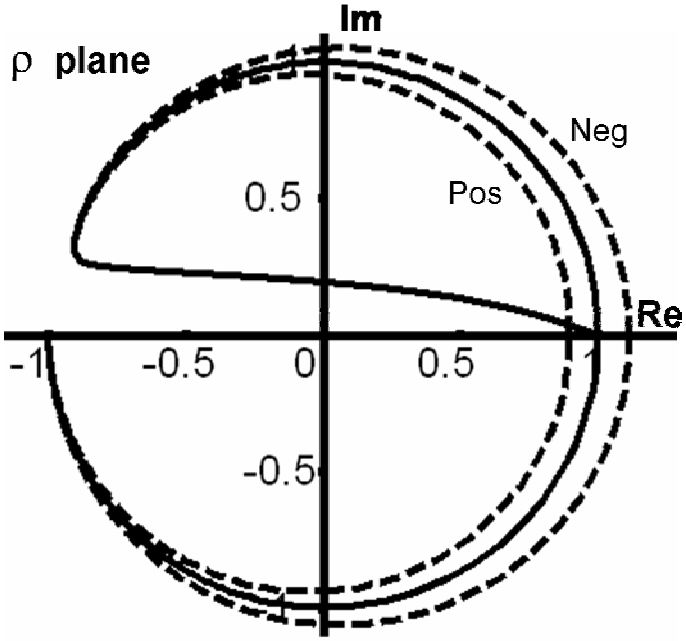

Figure 3.7.3.1 Negative and Positive systems near the zero system exhibit similar behavior for PMJ designs. The design shown here is the 5° design for system 1 listed in Table 3.7.1. The slightly negative and positive systems for the film index sensitivity are shown dashed; the film index has been changed to the corresponding values of N_1 listed in Table 3.7.3.1.

Table 3.7.3.1 The sensitivity of the example designs for N_1. Note that for higher values of PJA the ranges increase. Also note that the tolerances improve from system 1 to system 2 and from system 2 to system 3. –j is more sensitive to a change in N_1 than +j.

System	PJA (°)	+j N_1 min	+j N_1 max	+j N_1 Range	-j N_1 min	-j N_1 max	-j N_1 Range
1	5	1.099997	1.100003	6.3E-06	1.099997	1.100002	4.9E-06
	10	1.099981	1.100007	2.59E-05	1.099986	1.100006	2E-05
2	5	1.459965	1.460032	6.73E-05	1.459989	1.460011	2.25E-05
	10	1.459829	1.460099	0.00027	1.459953	1.460041	8.83E-05
	15	1.459512	1.460096	0.000584	1.459888	1.460079	0.000191
3	5	1.696946	1.69705	0.000104	1.696991	1.697009	1.76E-05
	10	1.696751	1.697168	0.000417	1.696966	1.697033	6.72E-05
	15	1.696333	1.697223	0.00089	1.696928	1.697066	0.000138

3.7.4 Substrate index

Similar to the film index, changes in the substrate index, keeping N_1 unchanged, cause a change from a zero to a negative or a positive system. Increasing N_2 results in a negative system where decreasing N_2 results in a positive system. Despite the change in system category, the negative and positive regions analyzed are very close to the zero system and thus still have PMJ designs, Fig. 3.7.4.1. The –j design point is more sensitive to a change in N_2 than the +j design point, Table 3.7.4.1. Thus, the sensitivity for the –j design point is the restricting case when considering changes in substrate index. That is, to maintain the desired performance of the device, the more restricting condition must be considered. A larger range of N_2 satisfies the approximation for systems with a higher value of N_1, but the range tapers off to the limit of N_1=2.12, Fig. 3.2.4.

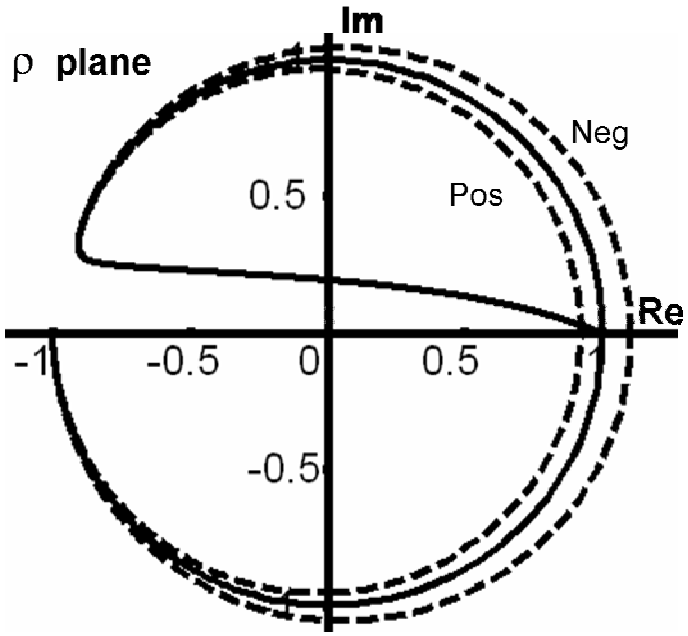

Figure 3.7.4.1 Negative and Positive systems near the zero system exhibit similar behavior for PMJ designs. The design shown here is the 5° design for system 1 listed in Table 3.7.1. The slightly negative and positive systems for the film index sensitivity are shown dashed; the substrate index has been changed to the corresponding values of N_2 listed in Table 3.7.4.1.

Table 3.7.4.1 The sensitivity of the example designs for N_2. Note that for higher values of PJA the ranges increase. Also note that the tolerances improve from system 1 to system 2 and from system 2 to system 3 with the exception of –j for the 15° design. –j is more sensitive to a change in N_2 than +j.

System	PJA (°)	+j N_2 min	+j N_2 max	+j N_2 Range	-j N_2 min	-j N_2 max	-j N_2 Range
1	5	1.209994	1.210008	1.39E-05	1.209995	1.210006	1.09E-05
	10	1.209985	1.210043	5.78E-05	1.209986	1.210031	4.45E-05
2	5	2.131492	2.131722	0.00023	2.131562	2.131639	7.71E-05
	10	2.131275	2.132212	0.000937	2.131461	2.131764	0.000303
	15	2.131306	2.133476	0.002171	2.131339	2.131999	0.000659
3	5	2.879585	2.880054	0.00047	2.879769	2.879848	7.94E-05
	10	2.879098	2.881003	0.001905	2.879661	2.879963	0.000303
	15	2.878948	2.883331	0.004383	2.879518	2.880142	0.000625

3.7.5 Design Performance

Reflected power is an important aspect of tunable retarder designs. Due to the low angles of operation and designs in SF2, reflectances for PMJ devices are low. This may be acceptable for some applications. For other applications, techniques may be used to increase the reflected power, for example by depositing a coating on the substrate to reflect light from the back of the substrate. Designs with higher values of N_1 produce higher reflectances, Table 3.7.5.1. Increasing PJA results in increasing $\Re_s$ and decreasing $\Re_p$, Table 3.7.5.1.

Table 3.7.5.1 Percentage reflected power for both p and s polarizations for the example designs. Note that the power for the two polarizations is almost equal; a result of the retarder approximation. For an exact retarder $\Re_p = \Re_s$.

System	PJA (°)	+j $\Re_p$	+j $\Re_s$	-j $\Re_p$	-j $\Re_s$
1	5	0.0087	0.0089	0.0087	0.0089
	10	0.0084	0.0093	0.0085	0.0092
2	5	0.1269	0.1287	0.1275	0.1281
	10	0.1241	0.1315	0.1266	0.129
	15	0.1195	0.1363	0.1252	0.1304
3	5	0.2291	0.2316	0.2301	0.2305
	10	0.2254	0.2353	0.2295	0.2311
	15	0.2193	0.2417	0.2287	0.2319

CONCLUSION

Film thickness subfamilies of film-substrate systems are discussed with an emphasis on subfamily 2 for retarder designs. Subfamilies are analyzed in the reduced film thickness plane, the film-thickness exponential function plane, and the ellipsometric function plane. By approximating the retarder condition, unique tunable retarder designs of relative phase shifts approaching 360° were realized. An algorithm was developed to design a tunable retarder/modulator with emphasis on ±90° phase shifts. This allows linearly polarized light at a polarization angle of 45° to be reflected as circularly polarized light of clockwise or counter-clockwise rotation by changing the angle of incidence. The direction of rotation could represent a 0 or a 1 in communications applications. Designs for a reflection-type film-substrate optical modulator/tunable retarder were carried out. In addition, design contours presented can be used for reference when designing a plus and minus j device. Increasing the film index, maintaining the zero system, causes several changes to the design contours: widening the contours, increasing the range of the angle of incidence for designs, increasing the difference between the angle of incidence for +j operation and that for –j operation. Sensitivity analyses to the angle of incidence, the film thickness, the film index, and the substrate index are presented. Systems with a higher film index and higher selected values of angle of incidence for +j operation have higher tolerances to all input parameters: angle of incidence, film thickness, film index, and substrate index. Systems with a higher film index have higher reflectances. The tolerances for –j operation are lower for all input parameters than +j and serve as the restricting case for film thickness, film index, and substrate index selections.

REFERENCES

1. William H. Hayt Jr. and John A. Buck, *Engineering Electromagnetics, 6th Ed.* (McGraw-Hill, Boston, 2001) Sec. 11.5.

2. John A. Buck, *Fundamentals of Optical Fibers* (Wiley, New Jersery, 2004) Sec. 1.5.3.

3. J. M. Bennet and H. E. Bennet, W. G. Driscoll and W. Vaughan, Eds., *Handbook of Optics* (McGraw-Hill, New York, 1975).

4. R. M. A. Azzam, A. R. M. Zaghloul, and N. M. Bashara, "Ellipsometric function of a film-substrate system: applications to the design of reflection-type optical devices and to ellipsometry," J. Opt. Soc. Am. **65**, 252-260 (1975).

5. A. R. M. Zaghloul, R. M. A. Azzam, and N. M. Bashara, "Design of film-substrate single-reflection retarders," J. Opt. Soc. Am. **65**, 1043-1049 (1975).

6. A. R. M. Zaghloul, R. M. A. Azzam, and N. M. Bashara, "An angle-of-incidence tunable, SiO2-Si (film-substrate) reflection retarder for the UV mercury line λ=2537Å," Opt. Comm. **14**, 260-262 (1975).

7. S. Kawabata and M. Suzuki, "MgF_2-Ag tunable reflection retarder," Appl. Opt. **19,** 484-485 (1980).

8. M. S. A. Yousef and A. R. M. Zaghloul, "Ellipsometric function of a film-substrate system: characterization and detailed study," J. Opt. Soc. Am. A **6**, 355-366 (1989).

9. A. R. M. Zaghloul, D. A. Keeling, W. A. Berzett, and J. S. Mason, "Design of reflection retarders by use of nonnegative film-substrate systems," J. Opt. Soc. Am. **22**, 1637-1645 (2005).

10. A. R. M. Zaghloul and M. S. A. Yousef, "Unified analysis and mathematical representation of film-thickness behavior of film-substrate systems," Appl. Opt. **45**, 235-264 (2006).

11. A. R. M Zaghloul, M. Elshazly-Zaghloul, W. A. Berzett, and D. A. Keeling, "Thin-film coatings - a transmission ellipsometric function approach: I. Nonnegative transmission systems, polarization devices, coatings, and closed-form design formulas," Appl. Opt. **45**, 8916-8931 (2006).